Cyclic Temperature Dependence of Electrical Conductivity in Polyanilines as a Function of the Dopant and Synthesis Method

Laura Horta-Romarís[1], María-José Abad[1], M. Victoria González-Rodríguez[1], Aurora Lasagabáster[1,2], Pedro Costa[3], Senentxu Lanceros-Mendez[3,4,5]*

[1] Universidade da Coruña, Grupo de Polímeros, Centro de Investigacións Tecnolóxicas, Campus de Ferrol, 15471 Ferrol, Spain.

[2] Dpto Química Orgánica I, Facultad de Óptica y Optometría, Universidad Complutense de Madrid, Arcos de Jalón 118, Madrid 28037, Spain.

[3] Center/Department of Physics, University of Minho, Campus de Gualtar, 4710-057 Braga, Portugal.

[4] BCMaterials, Parque Científico y Tecnológico de Bizkaia, 48160-Derio, Spain.

[5] IKERBASQUE, Basque Foundation for Science, Bilbao, Spain.

*Submitting and corresponding author:

María-José Abad López

e-mail: mjabad@udc.es

Universidade da Coruña, Grupo de Polímeros, Centro de Investigacións Tecnolóxicas, Campus de Ferrol, 15471 Ferrol, Spain.

Tel: 34-981 337 400 (3415/3414) Fax: 34-981 337 429

Abstract

Most of the studies dealing with polyanilines (PANIs) are focused on electrochemical polymerization; however, chemical polymerization is more suitable for largeï scale production. In order to develop commercially viable, clean, effective materials for thermal sensor devices, temperature dependent electrical response has been studied in PANIs obtained by simple, low-cost synthesis conditions, transferable to industrial processing. PANIs doped with HCl, dodecylbenzene sulfonic acid (DBSA) and sodio-5-sulfoisophtalic acid (NaSIPA) were prepared by chemical oxidative polymerization, through direct and indirect routes of synthesis. TEM images disclosed formation of nanorods and microfibrils. Microstructural analysis confirmed differences in doping level and crystallinity which were related with the PANI conductivity.

Two PANI-DBSA synthesized by direct and indirect methods, exhibit the best conductivity retention up to 150 ºC. In cyclic tests, they show excellent performance after 4 heating-cooling cycles up to 70 ºC. The amplitude of electrical response for

PANI-DBSA obtained by direct synthesis is twice the value of PANI-DBSA prepared by indirect route. Conversely, the latter displays slightly better repeatability due to its lower moisture content. This study suggests that both PANI-DBSA are suitable for use in electronic applications, under ambient conditions below 150 ºC, and are promising materials for temperature sensor applications.

Keywords

Polyaniline, NaSIPA, DBSA, electrical conductivity, heating-cooling cycles, ageing.

1. Introduction

In recent years, there has been increasing interest in the synthesis and application of conducting polymers [1]. Specifically, polyanilines (PANIs) are the subject of considerable attention owing to their unique electrical behavior, good environmental stability in doped and neutral states and simple synthesis [2].

PANI has a broad application range covering rechargeable batteries [3], data storage [4], corrosion protections [5], solar cell devices [6] and sensors [7-10], among others. Polyaniline is an excellent candidate for fabricating sensor devices due their intrinsic electrical properties. It possesses valuable characteristics such as reversible acid/base doping/dedoping chemistry, enabling control over properties (free volume, conformational changes, solubility, electrical conductivity and optical activity) which result in sensitive and rapid responses to specific analytes and/or environmental factors [9].

In order to develop thermal sensors, it is essential to understand the temperature dependence of the electrical conductivity. Thus, from a theoretical point of view, it is common practice to study the variation of conductivity with temperature in the range of ~50- 300 K to comprehend the mechanism of conductivity [11, 12]. Notwithstanding, in practice these devices are often applied at room temperate and above. As a result, the thermal stability of conductivity in the latter temperature range is critical. A greater number of factors should be considered as in these conditions different changes are taking place in the system like doping, dedoping (extrinsic), oxidation, chain scission, cross-linking and changes in crystal structure (intrinsic) [13]. In addition, the study of the thermal stability of polyaniline is essential to understand the effect of heat treatment on physical properties. Despite the number of studies focusing on the improvement of the electrical properties of PANI, those analyzing the influence of thermal aging on these properties are relatively scarce [13-17].

In this context, the main objective of this work is to develop reliable, eco-friendly and scalable synthetic routes for large-scale production of polyaniline intended for the manufacture of sensors, including thermal sensors. As the chemical oxidation of aniline is more suitable than electrochemical polymerization for bulk production [18-20], the first alternative has been investigated. Concerning the synthetic methods, the properties of polyaniline can be tailored through doping with a wide scope of dopants and using direct and indirect approaches.

Regarding direct synthesis, HCl has been chosen as inorganic dopant due to the ease of synthesis and high electrical conductivity [21]. Dodecylbenzene sulfonic acid (DBSA) has been selected among organic dopants owing to the well-known enhancement of processability, as DBSA acts both as dopant (DBSA bonded to PANI backbone) and plasticizer (DBSA in excess or free DBSA) [20].

Another option is to obtain a synergistic combination between the high conductivity of the inorganic dopant and the improvement in processability and thermal stability achieved with the organic dopant by an indirect synthetic route, known as *dedoping-redoping* [11]. In this option, polyaniline doped with HCl (PANI-HCl) is completely dedoped in aqueous NH_4OH solution and, subsequently, redoped with a second organic dopant. As second organic dopants, the bulky counterions DBSA and sodio-5-sulfoisophtalic acid (NaSIPA) have been used [11].

The polymers thus synthesized were characterized using transmission electron microscopy (TEM), Fourier transform infrared spectroscopy (FTIR), Elemental Analysis, X-ray photoelectron spectroscopy (XPS), X-ray diffraction (XRD) and Thermogravimetric analysis (TGA). Their room temperature electrical conductivity has been compared by the four probe technique and the effects of various dopants and synthetic routes on DC conductivity are discussed. Finally, thermal stability of the DC electrical conductivity was monitored at different heating conditions and through heating-cooling cycles to analyze the potential of PANIs as thermal sensors.

2. Experimental

2.1. Materials synthesis

Aniline and potassium peroxodisulfate (APS) were purchased from Fluka (Steinheim, Germany). Dodecylbenzensulfonic acid (DBSA) 70 wt.% solution in 2-propanol and 5-sulfoisophtalic acid sodium salt (NaSIPA) 95 wt.% were obtained from Sigmaï Aldrich (Steinheim, Germany), acetone was obtained from Scharlau (Sentmenat, Spain),

chloroform and methanol were supplied from Merck (Darmstadt, Germany). All the solvents and reagents except DBSA were at least of 99% purity. Water was purified on a Milli-QUltrapure 109 system (Millipore, Molsheim, France).

Table 1 summarizes the main synthesis conditions and the sample nomenclature. The preparation of PANI-HCl (P1) was adapted from the method described by Park et al [22]. Aniline and APS were dissolved separately in 0.5M aqueous HCl. The polymerization reaction was initiated by the drop wise addition of the oxidant during approximately 20 minutes. Afterwards, the reaction was allowed to proceed for 2 h under mechanic stirring (350 rpm) at room temperature. The precipitate was filtered under vacuum and washed with a mixture of 1:1 water:acetone. The PANI-HCl was obtained as a dark green powder after drying at 40 ºC in vacuum until constant weight.

The polymerization of polyaniline doped with DBSA (PANI-DBSA direct synthesis) (P2) was prepared according to the method described by Dopico et al [23].

For the indirect synthesis, PANI-HCl prepared as described in the preceding paragraph, was dedoped with 1M NH_3 for 2 h in ultrasonic bath, filtered under vacuum and washed with water until neutral pH. The resultant product was redoped with 1M DBSA in acetone and 0.5 M aqueous NaSIPA during 2h in ultrasonic bath leading to PANI-DBSA indirect synthesis (P3) and PANI-NaSIPA (P4), respectively. This indirect procedure has the advantage of avoiding chloroform (less environmentally-friendly) which is used in the direct polymerization of PANI-DBSA. The samples were washed with large volumes of acetone to remove excess free acids. Finally, the products were filtered under vacuum and dried in vacuum at 40 ºC for 2 days [11].

After polymerization, the polyanilines thus prepared were stored inside an opaque container in a desiccator, to protect them from light and moisture until tests execution.

Table 1. Experimental procedure for the synthesis conditions of doped PANI.

	Sample	**Dopant**	**$M:D_1:O:D_2$**	**T (ºC)**	**Addition dropwise speed**	**Stirring speed (rpm)**
PANI direct synthesis	**P1**	HCl	1 : 5.6 : 1.25	RT	>1 drop/sec	350
	P2	DBSA	1:3:1	0-5	<1 drop/sec	150
PANI indirect synthesis	**P3**	HCl-DBSA	1 : 5.6 : 1.25 : 5.6	RT	>1 drop/sec	350
	P4	HCl-NaSIPA	1 : 5.6 :1.25 : 2.8	RT	>1 drop/sec	350

2.2. Characterization

The transmission electron microscope (TEM, Jeol JEM 1010, 80 KV) was used to investigate the morphology of the powder samples dispersed in isopropanol.

Fourier transformed infrared (FTIR) spectra of the polymers in KBr pellets were recorded on a Bruker Vector 22 spectrometer. The spectra were collected from 4000 to 400 cm^{-1} with a 4 cm^{-1} resolution over 100 scans.

The elemental analysis of C, H, N, S was conducted using ThermoFinnigan FlashEA1112 elemental analyzer.

The XPS spectra were performed with a Thermo Scientific K-Alpha ESCA instrument with Al-KŬ monochromatized radiation at 1486.6 eV X-ray source, operated in a constant analyser energy mode (CAE) with 100 eV and 20 eV pass energy for survey and high resolution spectra, respectively. All core-level spectra were referenced to the C1s neutral carbon peak at 285 eV. The atomic concentrations were determined from the XPS peak areas using the Shirley background subtraction technique and the Scofield sensitivity factors. The N(1s), S(2p) and Cl(2p) peaks were deconvoluted into Gaussian\Lorentzian component peaks by the manufacturer (Thermofisher) software (Avantage version 5.47).

X-ray patterns of polyaniline powders were recorded in step-scan mode from 2º to 50º with a 2ɗ step of 0.05º using a D5000 diffractometer (XRD, Siemens- Bruker) with CuKα line irradiation (ə= 1.541 $x10^{-10}$m). 40-point smoothing protocol using a Savitzky-Golay filter has been applied to the diffractograms, which were normalized to area 1 (Origin 8.0 graphical software). A split Gaussian function was used to subtract the background and amorphous contributions using the open-source software Fityk. The difference patterns were deconvoluted into the crystalline constituents using Gaussian function peak shape approximation [24]. The degree of crystallinity (X_c) was estimated from the percentage of crystalline peak area to total scattered area, the d-spacing was calculated using the Bragg equation, the crystallite domain size (L) was evaluated using the Scherrer formula [25]. The interchain separation lengths (R) of the highest intense crystalline peaks were determined from the relation given by Klug and Alexander [26].

Thermogravimetric analysis (TGA) was performed with a Perkin-Elmer TGA-7 over a temperature range of 25ï 700 ºC, at a heat rate of 10 ºC/min under oxygen atmosphere.

Electrical resistivity was measured with a LORESTA-GP electrical analyzer (Mitsubishi Chemical, MCP-T610) on specimens prepared by compression molding (2.5x2.5 cm x 0.5 mm). The measuring range of this equipment lies between 10^{-2} - 10^{7} q.

Measurements were conducted at room temperature using a 4-point test fixture (gold contact wires with and inter-pin distance of 5 mm). The electrical conductivities reported (the inverse of electrical resistivity) for each polymer are the mean values of at least 24 readings determined on different probes.

The temperature dependence of the electrical resistance was measured under oxygen atmosphere with the digital multimeter Agilent 34401A (DC) in synchronization with the temperature control Linkam THMSE 600. The data were recorded every second for the different samples and temperatures ranges. Three different tests were performed: all samples were subjected to a heating ramp until 200 °C at 2 °C/min; besides, only P2 and P3 were subjected to a heating ramp until 350 °C at 10 °C/min and to heating-cooling cycles between 30 - 70 °C (5 °C/min).

In order to mimic the real working conditions of the material in sensor applications all the thermal tests were carried out under oxygen atmosphere.

3. Results and discussion

3.1. Morphological properties

The most noteworthy properties of polyanilines, in particular electrical properties, become dependent on their morphology, size and shape, when dimensions are decreased to the nanoscale. The TEM micrographs of the four PANI salts are presented in Figure 1. There are differences in the shape and size of the particles depending on the chemical nature of the dopant and the synthetic parameters. The particles of PANI-HCl (P1 in Figure 1A) and the polyanilines obtained by indirect synthesis (Figure 1C and 1D) are nanorod shaped. These nanostructures are fully appreciated on a larger scale in the insets of Figures 1A, C and D. By contrast, the P2 fibrils of Figure 1B, show micrometric dimensions.

Regarding P1, the rate of the aqueous polymerization at room temperature, with higher monomer:acid and monomer:oxidant ratios, is necessarily faster than the emulsion polymerization kinetic of P2 at 0-5 °C; thus, nucleation processes are favored over the polymer growth and explains the nanoscale morphology. Notwithstanding, the concentration of monomer and oxidant are low enough to produce nanorods in the presence of inorganic acids at extremely low pH values (pHå0), instead of the typical granular morphology, usually produced by the precipitation polymerization in strongly acidic media [27].

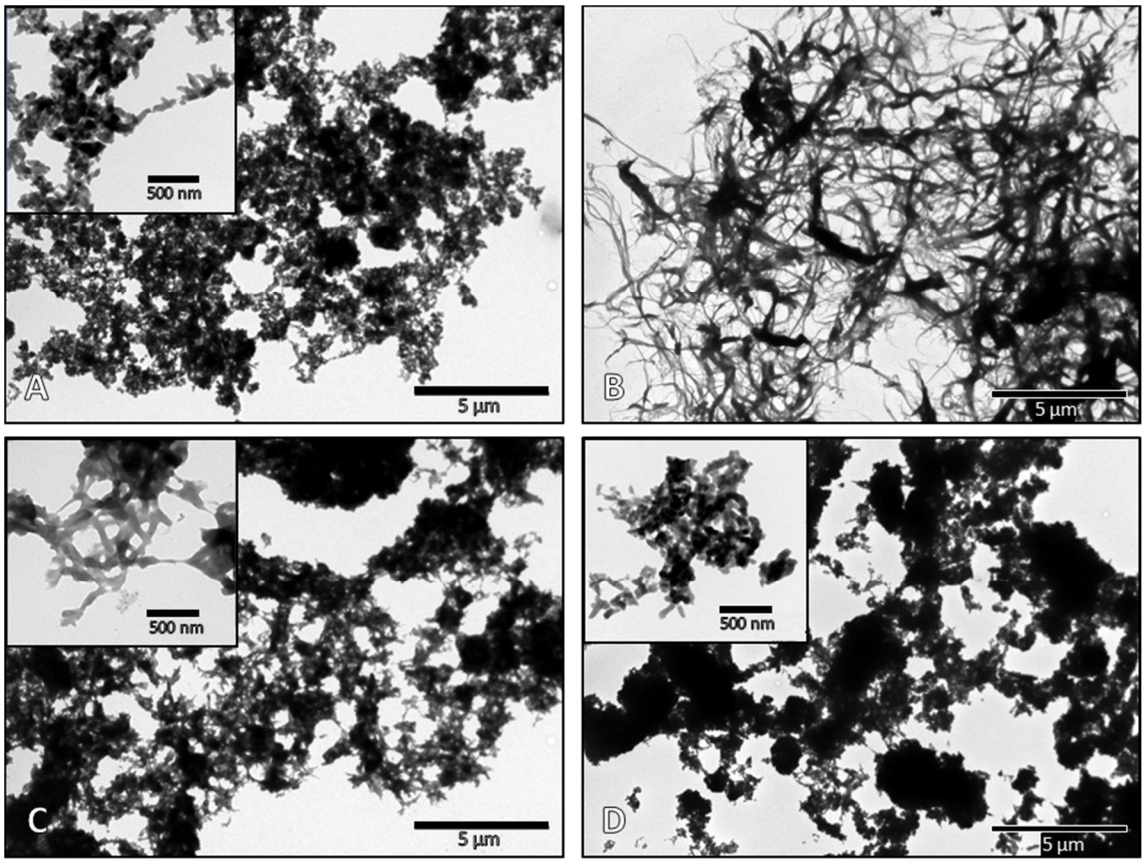

Figure 1. TEM images of the PANI samples showing their morphology: A) PANI-HCl (P1), B) PANI-DBSA direct synthesis (P2), C) PANI- DBSA indirect synthesis (P3) and D) PANI-NaSIPA (P4). The magnification is 6000x and the scale bar in the Figures is 5ε m. The insets magnification is 50000x and the corresponding scale bar is 500 nm.

On the other hand, P2 has been prepared by aqueous/organic interfacial polymerization in the presence of DBSA with lower aniline: acid and aniline: APS ratios and at lower temperature than the PANI-HCl. Several factors contribute to the microfibrillar morphology obtained by this procedure. First of all, the reactants and oligomeric intermediates are distributed between the aqueous and organic phases, creating the typical conditions of a dilution technique [28]. Secondly, the interface is expected to be crucial for the adsorption of nucleates and their organization rate [29]. In the third place, the low temperature further favors slow polymerization kinetics. Last, but not least, the pH profile is also relevant: weak organic acids bring the initial pH to the desired low-acidity level and further act as buffers, that resist the pH decrease caused by the produced sulfuric acid when APS is the oxidant [27].

In summary, all these experimental conditions promote that the aniline nucleates become organized to form one-dimensional stacks stabilized by π-π interactions

between phenazine-containing oligomers. Subsequently, polyaniline chains grow from the self-assembled nucleates leading to microfibrils. The growth of the microfibril is preferred over the start of new fibers [27].

In relation with redoped samples, both dedoping and redoping processes are influenced by the morphology of the pristine PANI-HCl. Not surprisingly, the morphology of P1 nanorods is hardly unaffected by the dedoping and redoping process in P4 (PANI-NaSIPA). By contrast, P3 (PANI-DBSA) shows intermediate morphology between P1 and P2 with longer, wider and more interconnected nanorods (Fig. 1C Inset). The surfactant nature of DBSA explains the observed differences. PANI aggregates are covered by a DBSA rich surface layer, which consists on fully doped PANI-DBSA and free DBSA (core/shell structure). The excess DBSA acts as a plasticizer and covers the conductive outer layer [30].

3.2. Chemical composition by FTIR, elemental analysis and XPS

The alternative arrangement of quinoid and benzenoid rings in PANI (half oxidized/half reduced emeraldine base (EB)) plays a significant role towards the achievement of high conductivity, creating chance for polaron formation in the presence of protonic acid, which is responsible for the conduction (Fig. 2A) [31]. Besides the oxidation state there are other factors which influence the conductivity of polyaniline such as the doping level and type of dopant, molecular weight, crystallinity and molecular arrangement [1].

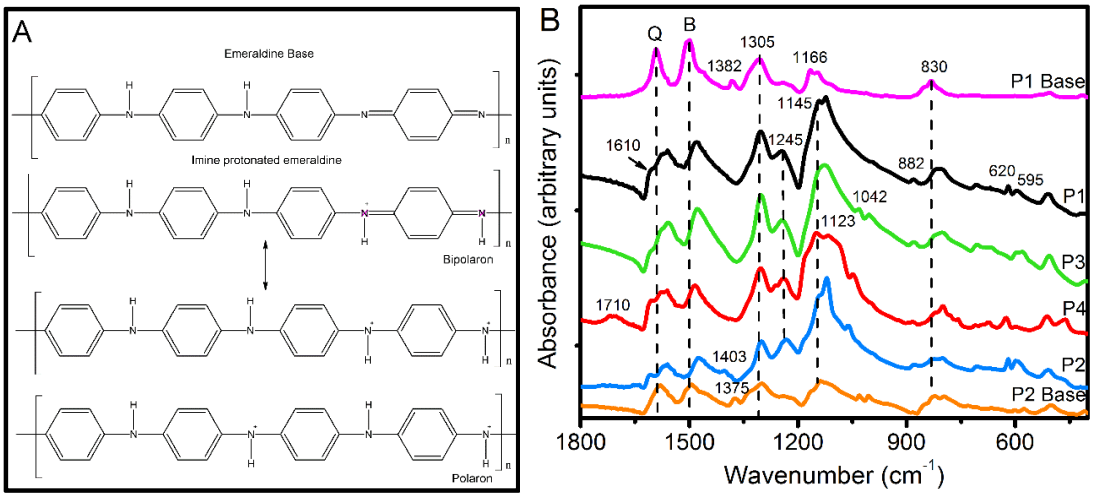

Figure 2. (A) PANI emeraldine base (EB) and its different protonated forms (B) FTIR spectra of PANI bases and PANI salts: PANI-HCl (P1), PANI-DBSA direct synthesis (P2), PANI-DBSA indirect synthesis (P3) and PANI-NaSIPA (P4).

3.2.1. FTIR

FTIR spectra of doped polyanilines and corresponding bases are depicted in Fig.2B in the range of 1800-500 cm^{-1} for the sake of clarity. The bands assigned to the quinoid (Q, $\nu_{C=N,\ C=C}$) and benzenoid (B, $\nu_{C=C}$) moieties are located at Q/B= 1561/1478 and 1564/1475 cm^{-1}, for P1 and P2, respectively. For both samples, the shoulder at ~1610 cm^{-1} is alloted to NH^+ deformations [32]. When PANI salts are treated with alkali, the Q and B modes upshift to 1591/1499 cm^{-1} for P1 base and to 1580/1493 cm^{-1} for P2 base while the shoulder at ~1610 cm^{-1} disappears. The new band at 1382 cm^{-1} for P1 base and 1375 cm^{-1} for P2 base, is typical of a standard PANI base (ν_{C-N} in the proximity of a quinoid ring) [33, 34].

The Q and B bands shift to 1559/1470 and 1561/1488 cm^{-1} upon redoping with DBSA (P3) and NaSIPA (P4), respectively. This implies that P3 is more protonated than P1 and P2 and that P4 is the least protonated sample [33].The intensity ratio of the Q/B absorption bands (I_Q/I_B) is indicative of the oxidation state of the polymer. A value of 1.0 defines the emeraldine type structure [21].The I_Q/I_B ratios are close to unity, indicating that PANI samples somewhat display an emeraldine form: 0.85 (P1), 0.78 (P2), 0.82 (P3) and 0.90 (P4). The oxidant concentration and the pH of the reaction medium are the key factors that influence oxidation [21]. The lower APS concentration used in the preparation of P2 compared to P1 may have favored the reduction state of polyaniline, whereas the different nature and/or concentration of the acids used for redoping explains the difference between P3 and P4.

The bands characteristics of the conducting protonated salt are observed at 1245 cm^{-1} (ν_{C-N+} in the polaron structure) and at 1145-52 cm^{-1} (combination of ŭ $_{C-H}$, ŭ$_{Q=N^+-B/\ B-NH^+.-B}$). The latter is considered a measure of the degree of electron delocalization and is characteristic of PANI conductivity. It is shifted to 1166 cm^{-1} in the P1 base ($\breve{u}_{C-H/N=Q=N}$) but no shift is detected in the P2 base [33]. The relative intensity of this peak compared to the ~1300 cm^{-1} band (ν_{C-N-C} of secondary aromatic amine) is considerably increased in the doped samples with respect to the emeraldine base.

The branching of PANI chains is an issue rarely mentioned that could negatively affect conductivity. The broad band at 825-830 cm^{-1} is related to aromatic C-H out-of-plane bending vibration (γ_{C-H}) on a 1,4-disubstituted aromatic rings. For branched PANI additional bands should be present at ~860 ($\gamma_{C-H1,2,4}$) and 760 ($\gamma_{C-H1,2}$) cm^{-1}. Since these

bands have not been observed, dominating p-coupling is confirmed. Thus, it is assumed that the PANIs are mainly linear. From another point of view, the spectrum of P2 contains a band at 1404 cm^{-1}, which has been related to the ring stretching of the phenazine unit, formed by oxidative intramolecular cyclation of o-couple aniline units or oxidative insertion of the aniline molecule in to p-linked aniline [33, 34].

Regarding the dopants, the characteristic absorptions of DBSA are observed for P2 and P3: the 2958, 2824 cm^{-1} and 2854 cm^{-1} bands ($\nu_{CH2asym,}$ $\nu_{CH2sym,}$) and the peaks 1042 and 1010 cm^{-1} ($\nu_{symO=S=O}$) [35, 36]. For P4, the bands of NaSIPA are located at 1710 cm^{-1} ($\nu_{C=O}$), 1042 cm^{-1} ($\nu_{O=S=O}$), 760 cm^{-1} (1, 3, 5- trisubstituted benzene ring of the dopant) and 624 cm^{-1} ($\check{u}_{SO3}$) [11].

As a final point, the spectra of the four doped polyanilines show bands at 882, ~620 and 595 cm^{-1} which have been assigned to S-OH or S-O-C stretching and S-O bending modes. The presence of HSO_4^-/HSO_3^- or SO_4^{-2} counterions in P1 is associated with the use of APS as oxidant and they can act as additional dopants [27, 34].These counterions are completely removed by deprotonation of P1 with ammonium hydroxide (P1 Base).

3.2.2. Elemental Analysis and XPS

The chemical composition analyses of polyaniline samples are determined utilizing both elemental analysis (Table S1) and XPS analysis (Table 2).

The best way to calculate the protonation degree is to quantify the various nitrogen species from the curve fitted XPS N1s core level spectrum [37]. PANI samples have been deconvoluted to four and five peaks depending on the sample. The peaks at 398.5 eV and 399.7 eV are related to undoped imine and amine groups, respectively. The peaks with binding energies >400 eV are attributed to the positively charged nitrogens (N^+). The positively charged nitrogen contribution to the total nitrogen content ($-N^+/N$) is the doping level or protonation degree [38].

The doping level values are 0.57, 0.49, 0.60 and 0.38 for P1, P2, P3 and P4, respectively Table 2). These results are coherent with the Q and B band shifts observed in the FTIR. Besides, within experimental error, the ï N^+/N values are equivalent to the S/N bulk ratios for the three samples doped with organic sulfonic acids: 0.46, 0.62 and 0.30 for P2, P3 and P4, respectively (Table S1). Hence, the elemental analysis can be used to estimate the extent of doping when organic sulfonic acids are used as dopant [39].

Nevertheless, the S/N surface ratios (Table 2) for DBSA doped samples, P2 and P3, are higher than the corresponding bulk ratios. These facts imply that considerable amounts of free DBSA molecules are concentrated at the surface. The difference between the bulk and surface values in P3 is nearly twice the difference found for P2, due to both the synthesis and washing procedures. Regarding the synthesis, the amount of DBSA in relation with aniline employed in the synthesis of P3 is higher than in P2 (Table 1); concerning the washing step, water: acetone 1:1 is used in P2 whereas acetone is employed in P3. It has been proved that water is able to remove DBSA from the sample surface to a greater extent than acetone [37]. In relation with P4, the level of protonation and the sulphonation degrees obtained by elemental analysis and XPS are identical within experimental error, suggesting that all NaSIPA molecules act as counterions and that there is not free NaSIPA. These results confirm the formation of a DBSA rich surface layer in P3 and explain the differences in morphology depicted in section 3.1 between P3 (interconnected nanorods) and P4 (nanorods).

From another point of view, the presence of sulfur in P1 supports the interpretation of the FTIR data which confirmed that P1 contains non-negligible amounts of HSO_4^- /HSO_3^- or SO_4^{-2} counterions due to the APS oxidant (S/N~0.17 on molar base at the bulk, Table S1, and 0.21 at the surface, Table 2). In agreement with the FTIR spectra, sulfur containing species are completely eliminated by neutralization with ammonium hydroxide (P1 base, Table S1).

Furthermore, the fraction of positively charged nitrogens in P1 is superior to the sum of the Cl/N and S/N contents. In order to find out the real contribution of the different dopants, the peaks due to chlorine Cl 2p (196.95 eV) and sulfur S 2p (167.46 eV) have been deconvoluted. The Cl 2p core level spectrum shows the presence of two doublets at 198.0 and 200.5 eV attributed to the chloride anion and covalent chlorine, respectively [40]. Likewise, the S 2p spectrum has been fit using two doublets at 168.8 and 170.25 eV. The doublet with lower binding energy is assigned to the sulfur of the sulfonate or sulfate group, which acts as a counter ion, and the doublet with the higher binding energy is from the sulfur in neutral sulfonic or sulfate acid [41]. Based on the precedent assignments, it is found that ~74.16% of Cl and ~67.23% of S present protonate the PANI. The remaining ~25.84% Cl and ~32.77% S are in neutral form. Combining with the total Cl and S the doping percentages convert to molar ratios, [Cl^- /N] and [HSO_4^-, HSO_3^- or SO_4^{-2}/N] (Table 2). The sum of the latter, equal to 0.28, is

considerably less than the degree of protonation ($-N^+/N$= 0.57), implying that water plays an essential role in protonation. This observation is coherent with the weight loss at low temperature calculated by TGA in section 3.5. More to the point, the XPS Cl/N ratio of 0.19 is surprisingly low. The extremely low Cl/N ratio was already observed by other groups for PANI and attributed to the surface oxidation or to the purification method [42].

Similarly, the S2p spectra of P2 and P3 were fit using two doublets. The doublet with lower binding energy is assigned to the sulfur of the sulfonic group (SO_3^-, 168.0 eV) (Area% = 51 and 34.46, for P2 and P3, respectively) and the doublet at 168.85 eV allotted to the neutral HSO_3 form (Area% = 49 and 65.55, for P2 and P3, respectively). Combining with the total sulfonation levels of Table 2 convert to [SO_3^-/N] molar ratios, 0.36 and 0.37 for P2 and P3, respectively. In both cases, the N^+/N ratio exceeds the [SO_3^-/N] ratio. This fact implies that water may also play a role in protonation. This outcome is consistent with the water loss at low temperature calculated for P2 by TGA analysis in section 3.5 but not with the water content of P3. Nevertheless, it must be born in mind that the XPS technique is sensitive to the very surface (~5 nm depths) and sometimes the results may not be reliable to obtain information of the bulk sample [42].

Table 2. XPS surface compositions (atomic percentage), doping levels and electrical conductivity of PANI salts.

	N1s Core level spectrum			XPS Stoichiometric totals					Conductivity
Sample	=N-/N	NH/N	$-N^+$/N	S/N	Cl/N	C/N	SO_3^{-2}/N	Cl^-N	σ (S/cm)
P1	0.05	0.38	0.57	0.21	0.19	6.58	0.14	0.14	14.7±1.8
P2	0.06	0.45	0.49	0.71	-	16.15	0.36	-	7.7±1.1
P3	0	0.40	0.60	1.07	-	21.13	0.37	-	9.9±0.6
P4	0.07	0.55	0.38	0.33	-	8.32	-	-	3.9±0.3

3.3. X-ray diffraction studies

The crystallinity and orientation of conducting polymers have been of much interest because highly ordered systems can display metal-like conductive states [25]. The powder XRD patterns of the four polyaniline salts together with the emeraldine base (P1 base) are shown in Figure S1. The *d*-spacings, interchain separation, normalized

intensity and crystallite size for the main peaks together with the degree of crystallinity are displayed in Table 3.

Table 3. The *d*-spacing, relative intensity, interchain separation, crystallite size and degree of crystallinity (X_c) of the four PANI salts.

Sample	**2ɗ** (°)	**I**	**d** (x10^{-10}m)	**R**(x10^{-10}m)	**L** (x10^{-10}m)	**X_c (%)**
P1	9.38	0.005	9.42	11.80	-	**29**
	15.10	0.010	5.86	3.63	-	
	20.55	0.011	4.32	5.40	-	
	25.65	0.046	3.47	4.34	44	
P2	9.68	0.004	9.13	11.41	-	**48**
	14.97	0.026	5.91	2.36	-	
	19.95	0.032	4.45	5.56	-	
	25.30	0.069	3.52	4.40	86	
P3	2.70	0.028	32.30	40.4	54	**14**
	19.15	0.017	4.63	5.79	-	
	25.33	0.009	3.51	4.39	-	
P4	15.02	0.011	5.90	1.76	-	**16**
	19.95	0.014	4.45	5.57	-	
	25.15	0.025	3.54	4.43	49	

The two samples obtained by direct synthesis exhibit partial crystallinity although P2 has a higher degree of crystallinity than P1. Both samples show main reflection peaks at about 2ɗ å 15, 20, and 25.5 and small peaks at 9.4, 27.6, and 29.7°. The peaks at ~20º and 25.5º belong to periodicity parallel and perpendicular to polymer chain, respectively [43, 44]. As previously reported, these crystalline features can be indexed in a pseudo-orthorhombic cell and are indicative of partially crystalline emeraldine salt of ES-I form [25]. Dedoping of ES-I leads to the amorphous emeraldine base, EB-I, with a broad band at a 2ɗ value of ~ 19-20º [43].

The amorphous base becomes slightly crystalline when redoped with DBSA (P3) and NaSIPA (P4). P3 exhibits a sharp peak at 2ɗ= 2.7º together with amorphous scattering centered at 2ɗ=19.2º and some weak features at ~25º. The wide angle peak at ~19.2º may be the superposition of the amorphous scattering and disordering of the polyaniline

chains, whereas the peak at the low angle is a characteristic feature of an interlayer repeat [45]. P4 is isomorphous with respect to P1 and P2, with three broad Bragg peaks visible centered at 2ɗ ~ 15, 20 and 25.2 $x10^{-10}$m.

Except for P3, the highest relative intensity corresponds to the peak at 2ɗ~ 25.5 $x10^{-10}$m, increasing with the degree of crystallinity. The ranges of the interchain distances and crystalline domain sizes shown in Table 3 are in agreement with values previously reported [25]. The *d*-spacings and interchain distances of P1 are smaller than the values calculated for P2, despite the greater crystallinity degree and crystallite size of the latter, probably due to the size of the dopant. The compact structure of P1, with the smallest π-π stacking distance, may favor the interchain hopping in the polyaniline and consequently the charge carrier mobility [46, 47]. P3 and P4 interchain distances are closer to P2 or slightly higher.

As stated before, contrary to P2, P3 forms a lamellar type structure consisting of PANI chains with irregular conformations and elongated alkyl tails of the DBSA, which function as spacers with some degree of interdigitation between parallel planes or sheets stacked by polymer backbones. This layered structure has been extensively described for DBSA-doped samples, especially for polymers prepared by indirect synthesis [45, 48]. The layer to layer distance, which can be determined from the smaller diffraction angle at 2.7 $x10^{-10}$m (d= 32.3 $x10^{-10}$m), is proportional to the size of the spacers and influenced by the doping level. The domain size of the layered structure regions, estimated from the width of the small angle peak, is 54 $x10^{-10}$m. The anisotropic orientation of the dopant alkyl chains can not only promote interchain diffusion of carriers but also optimize transportation within individual layer [45].

3.4. Thermal behavior

Figure 3 displays the thermal behavior of doped PANIs evaluated by Thermogravimetric analysis (TGA). The four PANI salts show weight losses at low temperature, due to solvent evaporation and release of volatile components. Directly doped polyanilines samples, P1 and P2, exhibit water contents around 10%, whereas redoped PANIs have lower water contents, 2.6 and 5% for P3 and P4, respectively. The electrical conductivity of polyaniline with water content between 10-20% may be affected by the moisture removal on heating [49].

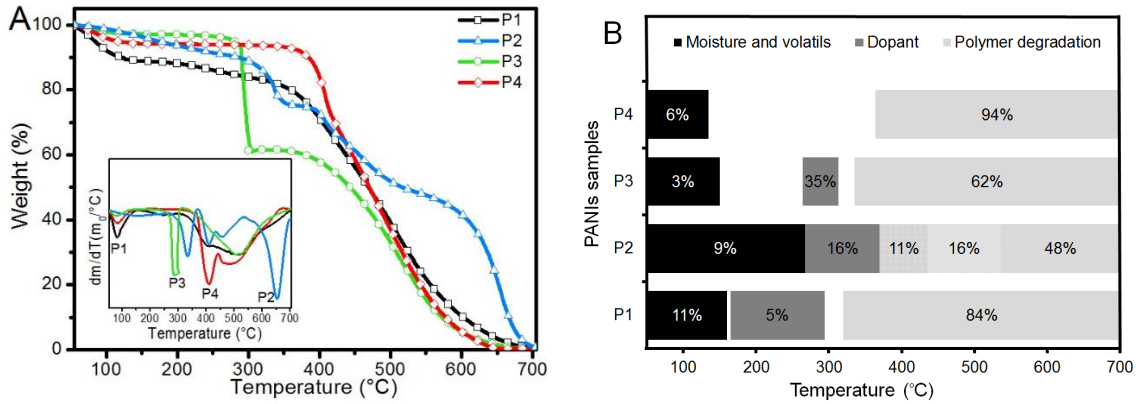

Figure 3. TGA and DTG curves (A) and temperature intervals with corresponding weight losses for the different degradation events (B) of PANI-HCl (P1), PANI-DBSA direct synthesis (P2), PANI-DBSA indirect synthesis (P3) and PANI-NaSIPA(P4) samples from 35 to 700 ºC at 10 ºC/ min under oxygen atmosphere.

Concerning P1 degradation, there are three steps in the thermogram of Figure 3 while the P1 base has only two steps (not shown). The second step, which is related to the loss of HCl acting as dopant and probably to HSO_4^- / HSO_3^- or SO_4^{-2} counterions produced from APS (minimum of the second weight loss in the first derivative thermogram ~245ºC), is absent in the degradation curve of the emeraldine base [50]. The third step, identified above 320 °C, is attributed to the actual decomposition of polyaniline. The first derivative plot of P1 shows a shoulder around 410 °C. It has been ascribed to the loss of bound HCl from deep inside the bulk of the polymer clusters, followed by degradation of the polymer chains at higher temperatures, as it is missing in the corresponding first derivate plot of the P1 base [32].

Likewise, the thermogram and derivative curve of P2 have been compared with the corresponding base (not shown). After the usual loss of solvent and volatiles, the dopant degradation occurs (second step). A 6% weight loss is also detected in this range for the P2 base, confirming the presence of a small amount of DBSA, previously observed by FTIR. Within the third step, two stages are observed in both P2 and P2 base. The one spanning from 370 to 536 ºC shows two unresolved peaks in the first derivate plot. They have been tentatively related with oxidation reactions, as they have not been observed under nitrogen atmosphere [35], and/or possible oligomers degradation, owing to the presence of phenazine-containing aniline oligomers detected by FTIR spectroscopy. Finally, the heavy weight loss over 537°C is ascribed to the breaking down of the polymer backbone.

In relation to P3, the significant weight loss in the second step is attributed to the evaporation and degradation of the dopant. Above 400°C, the polymer degradation occurs. The minimum of the second weight loss in the first derivative thermogram is significantly shifted to lower temperature with respect to P2 (335 and 287 ºC for P2 and P3, respectively, Fig. 3A inset) and the weight loss is increased (Fig. 3B). The lower degree of crystallinity of P3 explains the decreased thermal stability in the second temperature range. It would need more energy for the dopant to be removed if the PANI chains are well arranged in a crystalline structure like in P2 [51].

Regarding P4, the first weight loss is due to bound and free water, whereas the weight loss over 371 °C involves the degradation of both NaSIPA dopant and the polymer (the derivative weight curve shows two unresolved minima at 410 and 490 °C, respectively). P4 has higher thermal stability than the two PANI-DBSA despite the lower degree of crystallinity compared with P2, owing to the superior thermal stability of the dopant [11]. DBSA decomposes about 250 ºC [49] whereas the degradation of NaSIPA starts around 440 ºC [11].

3.6. Thermal stability of DC conductivity

The room temperature conductivity of the four doped-PANI samples has been measured by the four-point probe technique (Table 2). As expected, the largest electrical conductivity at room temperature corresponds to P1 (ů = 14.7 S/cm) whereas P2 exhibits approximately half this value (ů = 7.7 S/cm). In addition to the inorganic nature of the dopant, the greater oxidation state, higher doping level and inferior π-π stacking distance between polyaniline chains, account for the superior conductivity of P1 with respect to P2 despite the lower degree of crystallinity of the former. Moreover, the presence of phenazine containing oligomers in P2 negatively affects the electrical conductivity, as they do not contain any extended conjugated system of double bonds, although they may simultaneously favor the chain alignment.

In relation with P3, the dedoping-redoping approach together with a molar aniline: DBSA ratio (1: 5.6) higher than P2 (1: 3), gives a polyaniline with intermediate properties between P1 and P2. The electrical conductivity of P3 (ů = 9.9 S/cm) is improved with respect to P2 due to the superior oxidation state and doping level, absence of oligomers and to the formation of a layered structure. It has been stated that the improvement of electric properties are assisted by the formation of the layered structures [45].

On the other hand, P4 shows the lowest conductivity of the four samples (ů = 3.9 S/cm). This value, lies between the conductivities obtained by Saini et al. [11] for directly and indirectly NaSIPA-doped PANIs. Despite the fact that P4 has the same nanorod morphology than P1 and the oxidation state of the emeraldine structure, the low conductivity is mainly ascribed to the small doping level and the low crystallinity without layered structure.

Furthermore, for the three samples doped with organic sulfonic acids the doping levels (ï N^+/N) values are equivalent to the S/N bulk ratios and the conductivities at room temperature are proportional to the doping levels (R^2= 0.95).

From another point of view, the thermal stability of the electrical conductivity strongly depends on moisture content, the chemical nature of the dopants and the crystal structure. Figure 4A shows that P2 relative conductivity remains practically constant upon heating from 25 to 200 ºC at 2 ºC/min, whereas P1 conductivity sharply decreases after 50 ºC, followed by P4 and the gradual loss of P3.

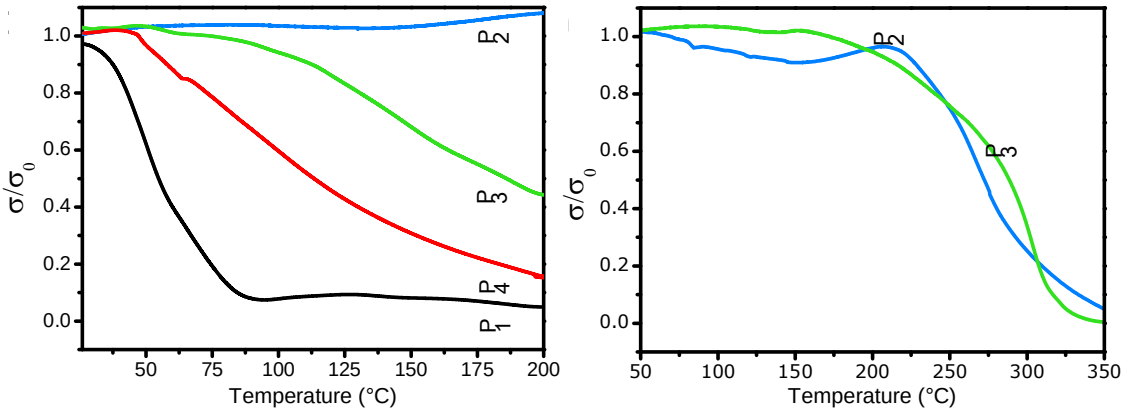

Figure 4. DC conductivity behavior as a function of temperature: A) from 25 to 200 °C at 2 ºC/min for PANI-HCl (P1), PANI-DBSA direct synthesis (P2), PANI-DBSA indirect synthesis (P3) and PANI-NaSIPA (P4) samples. B) from 50 to 350 °C at 10ºC/min for P2 and P3 samples.

Many studies have reported that organic acid doped polyanilines exhibit better conductivity retention compared to inorganic acid doped ones. For dopants with low molecular weight, such as HCl, the conductivity is lost even at temperatures as low as 50°C due to loss of moisture and dopant. Chlorine counterions and water can be easily extracted and evaporated from the polymer and dedoping destroys the crystal structure,

leading to the amorphous non-conductive emeraldine base [49, 52, 53]. The crucial role of water in the protonation of P1 has been proved by XPS and TGA analysis.

In contrast, large size organic dopants such as DBSA or NASIPA are not easily removed from the polymer matrix below 250 ºC, as described in the TGA analysis. Therefore, the dopant evaporation and degradation is not the main cause of the large reduction of the electrical conductivity of the P3 and P4 samples below 200 ºC at 2 ºC/min (Figure 4A). Besides, the moisture contents of these samples are lower than that of P2. To check the chemical changes of P3 and P4 due to the heating process, the FTIR spectra before and after heat treatment up to 230 ºC have been compared (not shown). The DBSA, NaSIPA and PANI characteristics bands remain unchanged. The only differences detected are a small decrease in the Q/B peak intensity ratio and the shift of the Q and B ring stretching bands to higher wavenumbers. These facts suggest that cross-linking reactions may have taken place and some of the acids have been transformed back to the undoped forms, respectively [35, 47, 52].

A noteworthy point is the difference in the thermal stability of conductivity between the two DBSA doped polyanilines, P2 and P3, which is probably due to structural differences, reflected by dissimilar morphologies, X-ray diffraction patterns and TGA profiles. The experimental conditions of direct emulsion polymerization promotes crystallinity and microfibrillar morphology [54]. The higher degree of crystallinity of P2 compared to P3 favors thermal stability as the aging process first affects the most disordered regions between the crystallites [14]. By contrast, the indirect approach achieves doping by introducing the DBSA (solved in acetone) into the solid, non-conducting amorphous emeraldine base, leading to low PANI crystallinity with a layered structure. It should be kept in mind that the real structure of this doped PANI is rather distorted and should better be considered in terms of a liquid ï like short range order [55].

Moreover, the thermal stability of P3 conductivity significantly improves up to 150 ºC at a heating rate of 10 ºC/min. This behavior has not been observed for P4 (not shown), which also has low crystallinity but no layered structure nor a surface shell of free dopant. From another point of view, in these conditions, P3 conductivity is less affected by moisture removal than P2 conductivity in agreement with the TGA results (Fig. 3B).

Anyway, direct and indirect synthesis using DBSA lead to samples with large thermal stability of the electrical conductivity. Due to the poor conductivity retention with

temperature observed for P1 and P4, these samples cannot be considered for thermal sensor applications.

Cyclic ageing studies have been further performed with P2 and P3. The results of four heating/cooling cycles from 30 to 70ºC at 5 ºC/minute are depicted in Fig 5. The amplitude of the electrical response of P2 is twice the value of P3 ($(\varphi\sigma/\sigma_0)/\varphi T$ are ~0.02 and ~0.01 for P2 and P3, respectively). Both materials exhibit good repeatability although a small loss in the relative conductivity of P2 is observed at the end of the fourth cycle of 2.79%, the sharpest drop occurring in the first two cyles. This trend may be explained by the release of moisture or volatile components [16]. Regarding P3, there is a negligible increase in the relative conductivity of 0.31% at the end of the experiment.

More to the point, P2 and P3 exhibit reverse behavior in each cycle. P2 increases the electrical conductivity with temperature (and vice-versa), while P3 shows a decrease in electrical conductivity with increasing temperature. The conductivity variation of P2 may be explained by the thermal doping concept (Fig. 5A). Owing to the presence of free DBSA molecules entangled at the surface, with the increase in temperature more DBSA can be doped into polyaniline by thermally enhanced mobility [14, 48, 49].

The thermoreversibility of P3 (Fig. 5B) is believed to be due to the lamellar type structure under the doped condition. Upon heating until 70º, the ionic bonds between the PANI iminic nitrogens and DBSA sulfonic groups break down which together with the disruption of the extended tails of the dopant mesomorphic structure leads to reduction of electrical conductivity; on cooling, the ionic bonds and the layered structure can be formed again and eventually the original conductivity is restored [56].

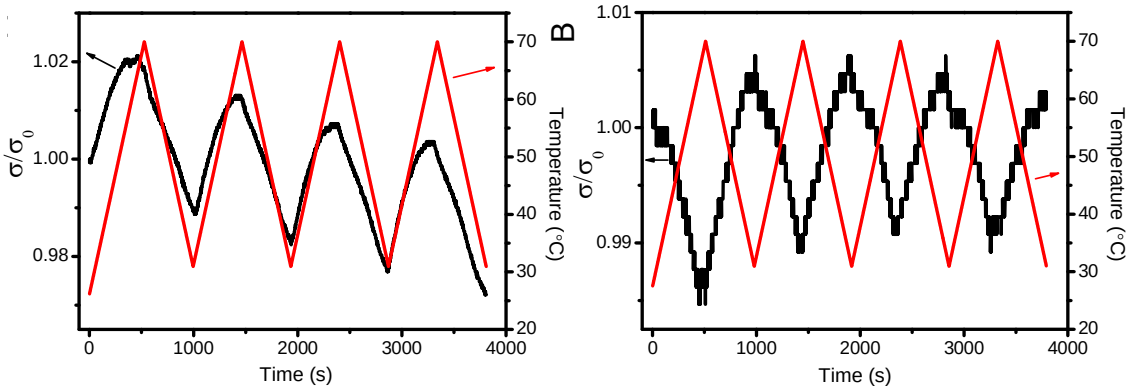

Figure 5. Cyclic temperature dependence of the DC electrical conductivity between 30 to 70 ºC for A) PANI-DBSA direct synthesis (P2) and B) PANI-DBSA indirect synthesis (P3).

Conclusions

In the current study, simple, low-cost synthesis methods, scalable to industrial volumes, are presented in order to obtain PANIs suitable for use in electronic applications. Initially four doped polyanilines samples have been prepared by chemical oxidative polymerization using two different routes including direct doping with HCl and DBSA and a dedoping-redoping approach with DBSA and NaSIPA.

The different routes of synthesis and experimental conditions lead to dissimilar morphology, structural order, oxidation state, doping level and thermal degradation profiles, which help to explain the conductivity values and the thermal stability of conductivity.

PANI-DBSA obtained by direct synthesis exhibits microfibrillar morphology and the highest crystalline level, although, the presence of phenazine oligomers may be responsible for the electrical conductivity value, which is lower than expected. All other polyanilines are nanorod shaped and have poor structural order.

As expected, PANI-HCl shows the highest electrical conductivity at room temperature but the worst conductivity retention in thermal assays. PANI-NaSIPA displays the smallest doping level plus low crystallinity, hence, the lowest conductivity of all. On the contrary, despite the low crystallinity level of PANI-DBSA obtained by the indirect method, the layered structured, observed in X-ray difractograms, together with its high doping level explain its high electrical conductivity. Besides, the indirect route of synthesis has the advantage of avoiding the use of chloroform (less eco-friendly).

Owing to superior conductivity retention with temperature, the two PANI-DBSA doped samples have been chosen for cyclic ageing studies. They both exhibit excellent electrical linearity and reversibility after 4 heating-cooling cycles up to 70 ºC. Regarding thermal sensitivity, the amplitude of the electrical response of PANI-DBSA prepared by direct synthesis is twice the value of PANI-DBSA obtained by the indirect route. In relation with repeatability, the former exhibits a small drop in relative conductivity (2.79%) at the end of the fourth cycle, assigned to its greater moisture content, whereas the latter displays a slight increase of 0.31%.

In summary, both kinds of DBSA doped polyanilines, which can be prepared by feasible routes for large-scale production, show potential for temperature sensor applications.

Acknowledgment

Authors acknowledge the financial support to Xunta de Galicia-FEDER (Program of Consolidation and structuring competitive research units (GRC2014/036)) and the FCT-Fundação para a Ciência e a Tecnologia for financial support under under Strategic Funding UID/FIS/04650/2013 and project PTDC/EEI-SII/5582/2014. Financial support from the Basque Government Industry Department under the ELKARTEK Program is also acknowledged.

References

[1] S. Bhadra, D. Khastgir, N.K. Singha, J.H. Lee, Progress in preparation, processing and applications of polyaniline, Prog. Polym. Sci. 34(8) (2009) 783-810.

[2] N. Su, Improving Electrical Conductivity, Thermal Stability, and Solubility of Polyaniline-Polypyrrole Nanocomposite by Doping with Anionic Spherical Polyelectrolyte Brushes, Nanoscale Research Letters 10(1) (2015) 1-9.

[3] F. Cheng, W. Tang, C. Li, J. Chen, H. Liu, P. Shen, S. Dou, Conducting Poly(aniline) Nanotubes and Nanofibers: Controlled Synthesis and Application in Lithium/Poly(aniline) Rechargeable Batteries, Chemistry ï A European Journal 12(11) (2006) 3082-3088.

[4] J. Huang, R.B. Kaner, Flash welding of conducting polymer nanofibres, Nat Mater 3(11) (2004) 783-786.

[5] B. Yao, G. Wang, J. Ye, X. Li, Corrosion inhibition of carbon steel by polyaniline nanofibers, Mater. Lett. 62(12ï 13) (2008) 1775-1778.

[6] M.-Y. Chang, C.-S. Wu, Y.-F. Chen, B.-Z. Hsieh, W.-Y. Huang, K.-S. Ho, T.-H. Hsieh, Y.-K. Han, Polymer solar cells incorporating one-dimensional polyaniline nanotubes, Org. Electron. 9(6) (2008) 1136-1139.

[7] I. Fratoddi, I. Venditti, C. Cametti, M.V. Russo, Chemiresistive polyaniline-based gas sensors: A mini review, Sensors and Actuators B: Chemical 220 (2015) 534-548.

[8] N. Chartuprayoon, M. Zhang, W. Bosze, Y.-H. Choa, N.V. Myung, One-dimensional nanostructures based bio-detection, Biosens. Bioelectron. 63 (2015) 432-443.

[9] J. Huang, S. Virji, B.H. Weiller, R.B. Kaner, Nanostructured Polyaniline Sensors, Chemistry ï A European Journal 10(6) (2004) 1314-1319.

[10] E. Falletta, P. Costa, C. Della Pina, S. Lanceros-Mendez, Development of high sensitive polyaniline based piezoresistive films by conventional and green chemistry approaches, Sensors and Actuators A: Physical 220 (2014) 13-21.

[11] P. Saini, R. Jalan, S.K. Dhawan, Synthesis and characterization of processable polyaniline doped with novel dopant NaSIPA, J. Appl. Polym. Sci. 108(3) (2008) 1437-1446.

[12] Z. Golsanamlou, M.B. Tagani, H.R. Soleimani, Improvement of thermoelectric efficiency of the polyaniline molecular junction by the doping process, PCCP 17(20) (2015) 13466-13471.

[13] S. Bhadra, D. Khastgir, Extrinsic and intrinsic structural change during heat treatment of polyaniline, Polym. Degrad. Stab. 93(6) (2008) 1094-1099.

[14] T. Chen, C. Dong, X. Li, J. Gao, Thermal degradation mechanism of dodecylbenzene sulfonic acid- hydrochloric acid co-doped polyaniline, Polym. Degrad. Stab. 94(10) (2009) 1788-1794.

[15] Z.A. ALOthman, M.M. Alam, M. Naushad, R. Bushra, Electrical Conductivity and Thermal Stability Studies on Polyaniline Sn (IV) tungstomolybdate Nanocomposite Cation-Exchange Material: Application as Pb (II) Ion-Selective Membrane Electrode, Int. J. Electrochem. Sci 10 (2015) 2663-2684.

[16] T. Anwer, M.O. Ansari, F. Mohammad, Dodecylbenzenesulfonic acid micelles assisted in situ preparation and enhanced thermoelectric performance of semiconducting polyanilineï zirconium oxide nanocomposites, Journal of Industrial and Engineering Chemistry 19(5) (2013) 1653-1658.

[17] N.G. Duran, M. Karakēda, L. Aksu, M. Saçak, Conducting polyaniline/kaolinite composite: Synthesis, characterization and temperature sensing properties, Mater. Chem. Phys. 118(1) (2009) 93-98.

[18] M. Jaymand, Recent progress in chemical modification of polyaniline, Prog. Polym. Sci. 38(9) (2013) 1287-1306.

[19] X. Li, Y. Wang, X. Yang, J. Chen, H. Fu, T. Cheng, Y. Wang, Conducting polymers in environmental analysis, TrAC Trends in Analytical Chemistry 39 (2012) 163-179.

[20] O.A. Araújo, M.-A. De Paoli, Pilot plant scale preparation of dodecylbenzene sulfonic acid doped polyaniline in ethanol/water solution: Control of doping, reduction of purification time and of residues, Synth. Met. 159(19ï 20) (2009) 1968-1974.

[21] T. Abdiryim, Z. Xiao-Gang, R. Jamal, Comparative studies of solid-state synthesized polyaniline doped with inorganic acids, Materials Chemistry and Physics 90(2ï 3) (2005) 367-372.

[22] H.-W. Park, T. Kim, J. Huh, M. Kang, J.E. Lee, H. Yoon, Anisotropic Growth Control of Polyaniline Nanostructures and Their Morphology-Dependent Electrochemical Characteristics, ACS Nano 6(9) (2012) 7624-7633.

[23] M.S. Dopico-García, A. Ares, A. Lasagabáster-Latorre, X. García, L. Arboleda, M.J. Abad, Extruded polyaniline/EVA blends: Enhancing electrical conductivity using gallate compatibilizers, Synth. Met. 189 (2014) 193-202.

[24] M. Wojdyr, Fityk: a general-purpose peak fitting program, J. Appl. Crystallogr. 43(5) (2010) 1126-1128.

[25] J.P. Pouget, M.E. Jozefowicz, A.J. Epstein, X. Tang, A.G. MacDiarmid, X-ray structure of polyaniline, Macromolecules 24(3) (1991) 779-789.

[26] X. Du, Y. Xu, L. Xiong, Y. Bai, J. Zhu, S. Mao, Polyaniline with high crystallinity degree: Synthesis, structure, and electrochemical properties, J. Appl. Polym. Sci. 131(19) (2014).

[27] J. Stejskal, I. Sapurina, M. Trchová, Polyaniline nanostructures and the role of aniline oligomers in their formation, Prog. Polym. Sci. 35(12) (2010) 1420-1481.

[28] N.R. Chiou, A.J. Epstein, Polyaniline Nanofibers Prepared by Dilute Polymerization, Adv. Mater. 17(13) (2005) 1679-1683.

[29] S. Palaniappan, A. John, Polyaniline materials by emulsion polymerization pathway, Prog. Polym. Sci. 33(7) (2008) 732-758.

[30] G.I. Titelman, A. Siegmann, M. Narkis, Y. Wei, Morphology of polyaniline redoped by kneading with dodecylbenzene sulfonic acid, J. Appl. Polym. Sci. 69(11) (1998) 2205-2212.

[31] A.G. MacDiarmid, ñSynthetic metalsò: A novel role for organic polymers (Nobel lecture), Angew. Chem. Int. Ed. 40(14) (2001) 2581-2590.

[32] A.V. Nand, S. Ray, M. Gizdavic-Nikolaidis, J. Travas-Sejdic, P.A. Kilmartin, The effects of thermal treatment on the antioxidant activity of polyaniline, Polym. Degrad. Stab. 96(12) (2011) 2159-2166.

[33] M. Trchová, I. ĠedĬnková, E. Tobolková, J. Stejskal, FTIR spectroscopic and conductivity study of the thermal degradation of polyaniline films, Polym. Degrad. Stab. 86(1) (2004) 179-185.

[34] M. Trchová, J. Stejskal, Polyaniline: the infrared spectroscopy of conducting polymer nanotubes (IUPAC Technical Report), Pure Appl. Chem. 83(10) (2011) 1803-1817.

[35] X. Lu, H.Y. Ng, J. Xu, C. He, Electrical conductivity of polyanilineï dodecylbenzene sulphonic acid complex: thermal degradation and its mechanism, Synth. Met. 128(2) (2002) 167-178.
[36] L.C. Costa, C.P.L. Rubinger, C.R. Martins, Dielectric and morphological properties of PAni-DBSA blended with polystyrene sulfonic acid, Synth. Met. 157(22ï 23) (2007) 945-950.
[37] G.M. Barra, M.E. Leyva, M.M. Gorelova, B.G. Soares, M. Sens, X-ray photoelectron spectroscopy and electrical conductivity of polyaniline doped with dodecylbenzenesulfonic acid as a function of the synthetic method, J. Appl. Polym. Sci. 80(4) (2001) 556-565.
[38] K. Neoh, E. Kang, K. Tan, Structural investigations of aromatic amine polymers, The Journal of Physical Chemistry 96(16) (1992) 6777-6783.
[39] P. Jayamurgan, V. Ponnuswamy, S. Ashokan, T. Mahalingam, The effect of dopant on structural, thermal and morphological properties of DBSA-doped polypyrrole, Iranian Polymer Journal 22(3) (2013) 219-225.
[40] K. Tan, B. Tan, E. Kang, K. Neoh, X-ray photoelectron spectroscopy studies of the chemical structure of polyaniline, Physical Review B 39(11) (1989) 8070.
[41] X.-L. Wei, M. Fahlman, A. Epstein, XPS study of highly sulfonated polyaniline, Macromolecules 32(9) (1999) 3114-3117.
[42] N. Kohut-Svelko, S. Reynaud, J. François, Synthesis and characterization of polyaniline prepared in the presence of nonionic surfactants in an aqueous dispersion, Synth. Met. 150(2) (2005) 107-114.
[43] A.R. Hopkins, R.A. Lipeles, S.-J. Hwang, Morphology characterization of polyaniline nano-and microstructures, Synth. Met. 158(14) (2008) 594-601.
[44] D. Bandgar, G. Khuspe, R. Pawar, C. Lee, V. Patil, Facile and novel route for preparation of nanostructured polyaniline (PANi) thin films, Applied Nanoscience 4(1) (2014) 27-36.
[45] W.-Y. Zheng, K. Levon, T. Taka, J. Laakso, J. Osterholm, Doping-induced layered structure in N-alkylated polyanilines, Polym. J. 28(5) (1996) 412-418.
[46] S. Hwang, W.J. Potscavage, R. Nakamichi, C. Adachi, Processing and doping of thick polymer active layers for flexible organic thermoelectric modules, Org. Electron. 31 (2016) 31-40.

[47] S. Bhadra, N.K. Singha, D. Khastgir, Dual functionality of PTSA as electrolyte and dopant in the electrochemical synthesis of polyaniline, and its effect on electrical properties, Polym. Int. 56(7) (2007) 919-927.
[48] K. Levon, K.H. Ho, W.Y. Zheng, J. Laakso, T. Kärnä, T. Taka, J.E. Österholm, Thermal doping of polyaniline with dodecylbenzene sulfonic acid without auxiliary solvents, Polymer 36(14) (1995) 2733-2738.
[49] S. Kim, J.M. Ko, I.J. Chung, Electrical conductivity change of polyanilineï dodecyl benzene sulfonic acid complex with temperature, Polym. Adv. Technol. 7(7) (1996) 599-603.
[50] X.L. Wei, Y.Z. Wang, S.M. Long, C. Bobeczko, A.J. Epstein, Synthesis and Physical Properties of Highly Sulfonated Polyaniline, J. Am. Chem. Soc. 118(11) (1996) 2545-2555.
[51] X. Zhang, J. Zhu, N. Haldolaarachchige, J. Ryu, D.P. Young, S. Wei, Z. Guo, Synthetic process engineered polyaniline nanostructures with tunable morphology and physical properties, Polymer 53(10) (2012) 2109-2120.
[52] A. Sobha, S.K. Narayanankutty, A promising approach to enhanced thermal stability of DC conductivity of polyanilineï functionalised multi-walled carbon nanotube composites, International Journal of Nanoparticles 7(2) (2014) 112-132.
[53] G. Ren, H. Qiu, Q. Wu, H. Li, H. Fan, C. Fang, Thermal stability of composites containing HCl-doped polyaniline and Fe nanoparticles, Mater. Chem. Phys. 120(1) (2010) 127-133.
[54] C.Y. Yang, P. Smith, A.J. Heeger, Y. Cao, J.E. Osterholm, Electron diffraction studies of the structure of polyaniline-dodecylbenzenesulfonate, Polymer 35(6) (1994) 1142-1147.
[55] W. Wernet, M. Monkenbusch, G. Wegner, A new series of conducting polymers with layered structure: Polypyrrole n-alkylsulfates and n-alkylsulfonates, Die Makromolekulare Chemie, Rapid Communications 5(3) (1984) 157-164.
[56] T. Jana, A.K. Nandi, Sulfonic acid-doped thermoreversible polyaniline gels: morphological, structural, and thermodynamical investigations, Langmuir 16(7) (2000) 3141-3147.